J. Phys. Res. Edu., Vol. 1, March 2024

A brief overview of Nanomechanical Qubits

Chandan Samanta*

Department of Physics, Indian Institute of Science Education and Research Bhopal, Bhopal-462066, Madhya Pradesh, India

Qubits are the building blocks for quantum computers and quantum information processing. However, there is a great deal of dispute over the most ideal types of qubits. The nanomechanical qubit might be one potential addition to the qubit platforms. Here, we briefly outline the underlying physical principle of a nanomechanical qubit, where the mechanical vibrations stores the information.

I. INTRODUCTION

Qubits serve as the fundamental units for quantum computers and quantum information processing. Research and development in this realm are rapidly progressing to determine which system or platform will emerge as the frontrunner. Among the array of possibilities are superconducting Josephson junctions[1, 2], semiconductor qubits [3–5], trapped ions [6–8], topological qubits [9, 10], ultra-cold neutral atoms [11, 12], and even diamond vacancies [13–15]. However, only a select few qubit platforms have thus far showcased the potential for quantum computing, meeting criteria such as high-fidelity controlled gates, effortless qubit-qubit coupling, and robust isolation from environmental interference, ensuring prolonged coherence. Nanomechanical resonators stand as a potential contender within this elite group of platforms. Over the past three decades, we have observed remarkable advancements in micro/nano-electromechanical systems [16–18]. This progress has led to technology that demonstrates exceptional performance across various applications, including sensing, imaging, timing, signal processing, and logic devices, among others. Moreover, these devices provide an intriguing opportunity to explore fundamental physics phenomena that include the quantum effects in macroscopic objects and the coupling of mechanical motion with photons, spins, and electrons.

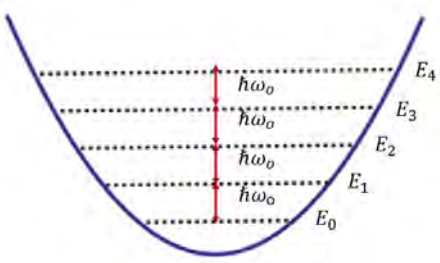

FIG. 1: The quantized energy levels of a simple harmonic oscillator having a frequency ω_0. The energy levels are evenly spaced.

A mechanical resonator is usually modeled as a harmonic oscillator. The energy of a simple harmonic oscillator can be written as $E_n = (n+1/2)\hbar\omega_0$, where $n = 0, 1, 2, ...$, $\hbar$ is the reduced Planck constant, and ω_0 is the resonance frequency of the oscillator. Here, $n = 0$ corresponds to the zero point energy with a corresponding fluctuation in displacement known as zero point displacement fluctuation $x_{\rm zp} = \sqrt{\hbar/(2m\omega_0)}$. This allows a mechanical resonator to be a test-bed for the quantum nature of macroscopic objects. There has been an intense effort to study mechanical resonators in the quantum regime. Several cool-down techniques have been implemented to achieve the ground state of a mechanical resonator. These devices are becoming a crucial new avenue in quantum science and technology. A plethora of proposals suggests their utility in storing, processing, and transducing quantum information. This requires progressively advanced methods to control mechanical motion within the quantum realm. These devices have been employed in achieving quantum ground state [19, 20], quantum squeezing [21–23], backaction-evading measurements [24, 25], entanglement [26, 27], coherent microwave-optical interface [28, 29], and superconducting qubit-mechanical interfaces [19, 30].

A recurrent question has been whether it is possible to realize strong nonlinearities in nanomechanical resonators approaching the quantum ground state. The origin of nonlinearity in case of large displacements is connected to the stress that depends nonlinearly on the displacement of a particular mode. It modifies the Hooks law as $F = -m\omega_0^2 x - \gamma x^3$ where γ is the the weak Duffing (or Kerr) constant and m is effective mass of the the mechanical eigenmode [31, 32]. The conventional devices are perfectly linear in the quantum regime. This means that the energy levels are equidistant. The vibrations in these resonators approaching the quantum ground state are only nonlinear at much larger values of x_{nl}, typically at $x_{nl}/x_{\rm zp} = 10^6$ or above. There have been efforts to introduce nonlinearity in mechanical resonators without much success. The proposition of anharmonicity resulting from proximity to a buckling instability has been made [33, 34]. Nevertheless, implementing such a scheme experimentally poses significant challenges.

Pistolesi *et al* [35] recently introduced a theoretical framework for a mechanical qubit utilizing the

coupling of one of the flexural modes of a carbon nanotube resonator to the charge state of a double-quantum dot defined in the same nanotube. It becomes feasible to generate adequate anharmonicity in the mechanical oscillator, enabling the coupled system to function as a mechanical quantum bit. Nevertheless, it is attainable solely when the device is operated in the ultrastrong coupling regime.

II. THE DEVICE AND THE ORIGIN OF ANHARMONICITY

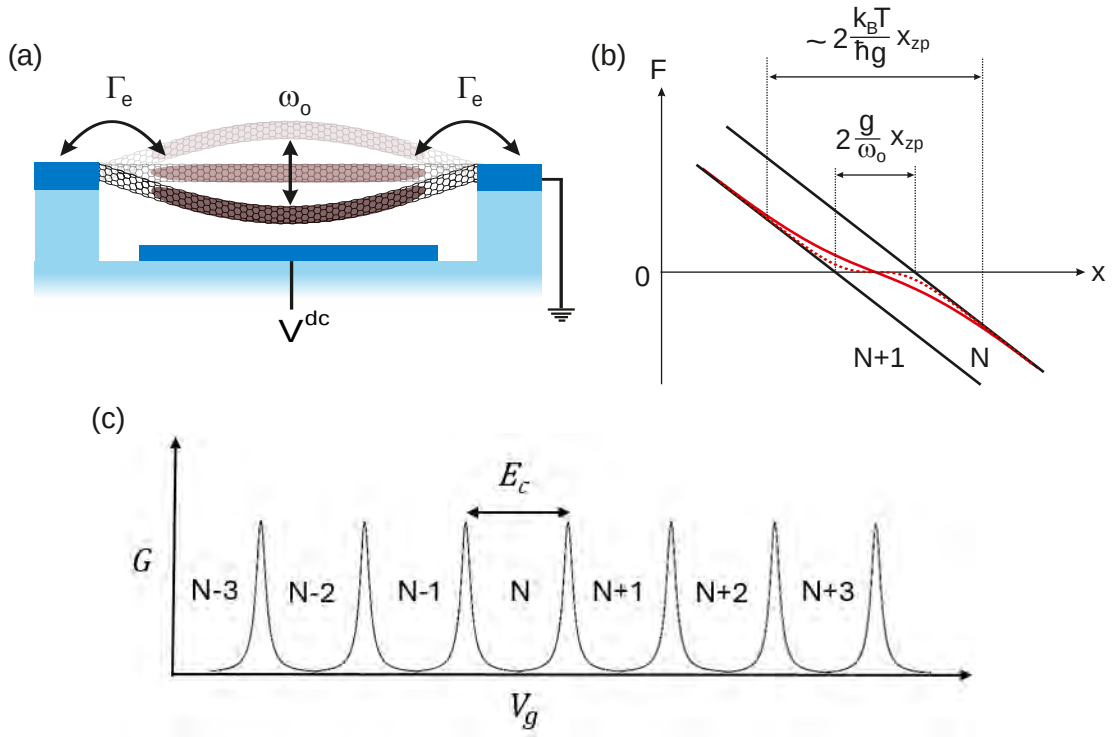

FIG. 2: (a) A schematic diagram that depicts the nanotube oscillating at ω_0. A quantum dot, shown in purple, emerges along the suspended nanotube, with an overall electron tunneling rate Γ_e to the left and right leads. (b) When the fluctuations between the two electron states are rapid compared to the mechanical motion ($\Gamma_e > \omega_0$), the force experienced by the vibrations is an average of the two linear F vs x curves (black straight lines) represents the situation in which the dot is filled with either N or $N + 1$ electrons weighted by the Fermi-Dirac distribution. The resulting force becomes nonlinear (shown in red) when the vibration displacement is smaller than $k_B T x_{zp}/(\hbar g)$. The reduced slope at zero displacement is a measure of the decrease in ω_0. As the temperature decreases, nonlinearity increases, as evidenced by the further reduction in slope at zero vibration, as depicted by the dashed red line. The separation between the two curves is $\Delta x = 2(g/\omega_0)x_{zp}$ due to the force generated by the electron tunneling onto the quantum dot. (c) A schematic of the conductance G as a function of the gate voltage.

Recently, there has been an experimental demonstration of a new mechanism to boost the anharmonicity of a carbon nanotube mechanical resonator [36]. This was achieved by coupling the resonator with single electron tunneling (SET) via a quantum dot non-resonantly. Figure 2(a) shows the schematic of a vibrating nanotube at a resonance frequency ω_0. The typical dimensions of the devices range from approximately $1-1.5$ μm in length, with a diameter of about 3 nm. The separation distance between the nanotube and the gate electrode is about 150 nm. A highly resistive silicon dioxide substrate with prepatterend source drain and gate electrodes were used to grow nanotube using chemical vapour deposition technique. The nanotube has a narrow band-gap and its electrochemical potential is tunable by underlying gate electrodes. The quantum dot is formed by creating a p-n tunnel junction at the ends of the suspended nanotube by applying a DC gate voltage. Figure 2(c) shows a simple schematic of gate voltage dependence of the conductance in the incoherent tunneling regime. This clearly indicates how a degenerate two-level system fluctuates between two states having N and $N+1$ electrons. The charging energy $E_c = e^2/C_\Sigma$ for the devices were about 8 meV, where e is electronic charge and C_Σ is the total capacitance of the quantum dot. A significant capacitive coupling was established between the nanotube island and the gate electrode by maintaining a minimal separation distance. This results in C_g being much greater than C_s and C_d, where C_s and C_d represent the capacitances between the nanotube island and the source and drain electrodes, respectively. The capacitance values were estimated by measuring the charge stability diagram of the quantum dot.

The resonator is coupled to the electrons within the dots through capacitive coupling between the nanotube and the gate electrode. This coupling can be described by the Hamiltonian $H = -\hbar g n_e x/x_{\rm zp}$, where g is the electromechanical coupling, and $n_e = 0, 1$ is the additional electron number in the quantum dot. Figure 2(b) describes the origin of nonlinearity in the mechanical resonator. The two black lines correspond to the linear force-displacement curves, when the dot is filled with either N or $N+1$ electrons, whose slopes are governed by the spring constant $m{\omega_0}^2$. The separation between two curves, $\Delta x = 2(g/\omega_0)x_{\rm zp}$, is caused by the force generated by one electron tunnelling onto the quantum dot. When the fluctuations between the two electron states are rapid compared to the mechanical motion ($\Gamma_{\rm e} > \omega_0$), the force experienced by the vibrations is simply an average of the two black force-displacement lines weighted by the Fermi-Dirac distribution. The resulting force (shown in red) is nonlinear when the vibration displacement is smaller than $\frac{k_B T}{\hbar g} x_{\rm zp}$. The reduced slope at zero vibration displacement is an indication of a decrease in ω_m. Here, T is the temperature, and k_B is the Boltzmann constant. If we decrease the temperature, the slope at zero point displacement is reduced further as shown by dashed red line in Fig. 2(b). The electron fluctuation rate is faster than the bare mechanical frequency i.e. ($\Gamma_e > \omega_0$) in the adiabatic limit. In this

case, the fluctuations result in the nonlinear restoring force as given by

$$F_{\text{eff}} = -\left[m{\omega_0}^2 - \frac{1}{4x_{\text{zp}}^2}\frac{(\hbar g)^2}{k_B T}\right] x - \frac{1}{48x_{\text{zp}}^4}\frac{(\hbar g)^4}{(k_B T)^3}x^3 \tag{1}$$

for $\Gamma_e < k_B T$ and $x \ll 2k_B T/\hbar g$.

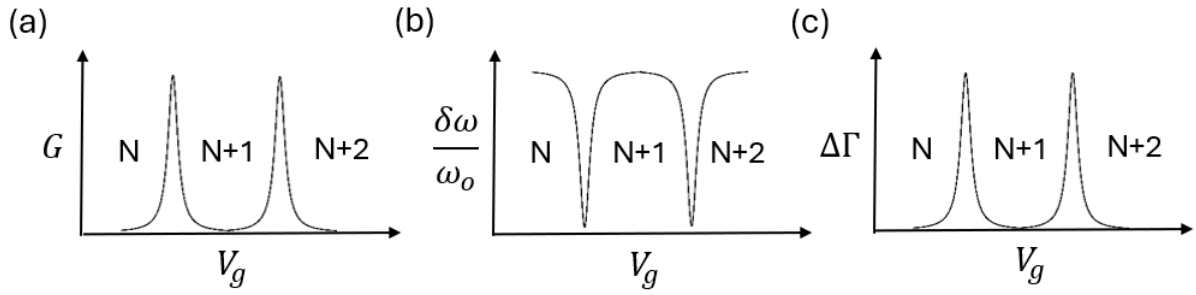

FIG. 3: (a) Schematic of conduction peaks with gate voltage in the SET regime. (b) and (c) represent schematics of change in resonance frequency and mechanical linewidth of the resonator across the conduction peaks, respectively.

Figure 3(b) illustrates the reduction of resonance frequency across the conduction peaks [shown in 3(a)] due to capacitive coupling between the mechanical vibration and the SET. Figure 3(c) shows a schematic of increase in linewidth Γ of the vibration across the conduction peaks [shown in 3(a)] due to incoherent tunneling of electrons between the dots and source/drain electrodes. A large number of experiments have been carried out [37–44], but the decrease in ω_0 has always been around 1% as the value of g was modest. The linear coefficient of the equation gives us

$$\omega_m = \omega_0\sqrt{1 - \frac{\varepsilon_p}{4k_B T}}, \tag{2}$$

where $\varepsilon_p = 2\hbar g^2/\omega_0$ is the polaronic energy. It is also clear that ω_m decreases with decreasing temperature. It was satisfactorily explaining the experimental observation. However, all the previous experiments could not be performed in a regime where $2k_B T \gg \hbar g^2/\omega_0$ due to lower values of g. This regime is referred as ultrastrong coupling regime, which can be realized in a mechanical system not in the ground state ($k_B T > \hbar\omega_0$) if $g > \sqrt{2}\omega_0$. It is also clear that ω_m vanishes when $2k_B T = \hbar g^2/\omega_0$ since the linear part of the restoring force vanishes as illustrated by the blue solid line in Fig. 4.

However, when we operate the device in the ultra-strong coupling regime, the nonlinear part dominates the dynamics of the resonator. The nonlinear force can even result in a vibration potential that is purely quartic in displacement. As a consequence of this nonlinearity, the oscillation period becomes highly dependent on the oscillation amplitude. Thermal fluctuations enable the oscillator to explore various amplitudes, resulting in different resonance frequencies. These fluctuations produce an observed resonance frequency that

is significantly higher than ω_m when averaged as shown in Eq. (2). The dashed red line in Fig. 4 depicts the theoretical prediction of the resonance frequency as a function of ϵ_p/k_BT incorporating both quartic nonlinearity and thermal fluctuations. This result was used to fit the temperature dependence of the resonance frequency at the conductance peak to estimate ϵ_p. The numerical result in Fig. 4 was fitted with the following analytical expression

$$\omega_m = \omega_0 \left[1 + \sum_{n=1}^{5} a_n \left(\frac{\epsilon_p}{k_B T} \right)^n \right] \tag{3}$$

with $a_1 = -0.127655$, $a_2 = 0.010475$, $a_3 = 0.0125029$, $a_4 = -0.00480876$, and $a_5 = 0.000515142$, which is within 0.1% of the numerical result for $0 \leq \frac{\epsilon_p}{k_B T} \leq 4$.

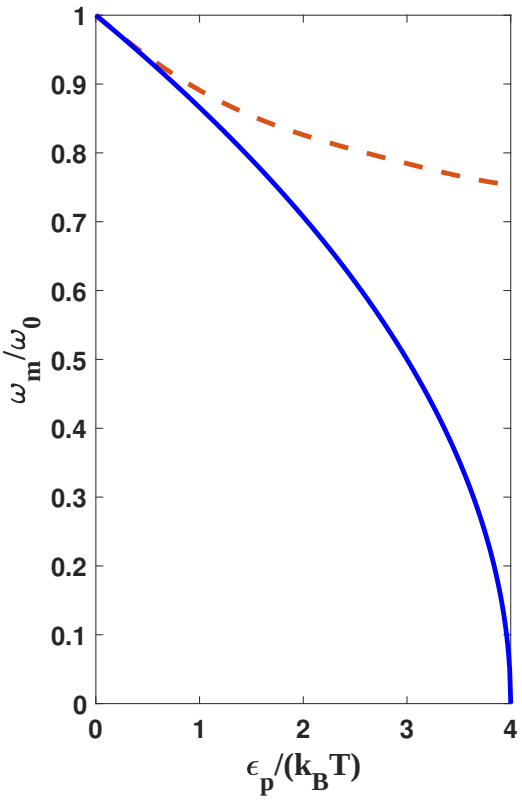

FIG. 4: The dashed red line illustrates the theoretical prediction for the renormalization of resonance frequency as a function of ϵ_p/k_BT, encompassing both quartic nonlinearity and thermal fluctuations. In contrast, the solid blue line represents the renormalization of resonance frequency excluding quartic nonlinearity and thermal fluctuations.

In contrast to earlier experiments, in Ref. [36], a substantial dip of approximately 25% in ω_0 was observed, along with an increase in the mechanical linewidth over 90% when the system was positioned on a conductance peak (Fig. 3), where the electronic two-level system reaches a state of degeneracy. Then, the authors repeated the measurements at different temperatures. The measured reduction in resonance

frequency as a function of temperature was then fitted using Eq. (3) to estimate the value of g. The largest value of the coupling strength g obtained from measurements was $g/2\pi = 0.5$ GHz. That corresponds to $g/\omega_0 = 17$. The value of g was consistent with the estimation $g/2\pi = 0.55$ GHz obtained from independent electron transport measurements. They used the formula $g = e(C'_g/C_\Sigma)V_g^{dc}/\sqrt{2m\hbar\omega_0}$, where m is estimated from driven spectral response measurements [45]. The spatial derivative of the dot-gate capacitance C'_g and the total capacitance C_Σ of the quantum dot were obtained from charge stability diagram of the device in the SET regime. These measurements established that the system was deep in the ultrastrong coupling regime.

III. FUTURE DEVICES AND EXPERIMENTAL PLAN

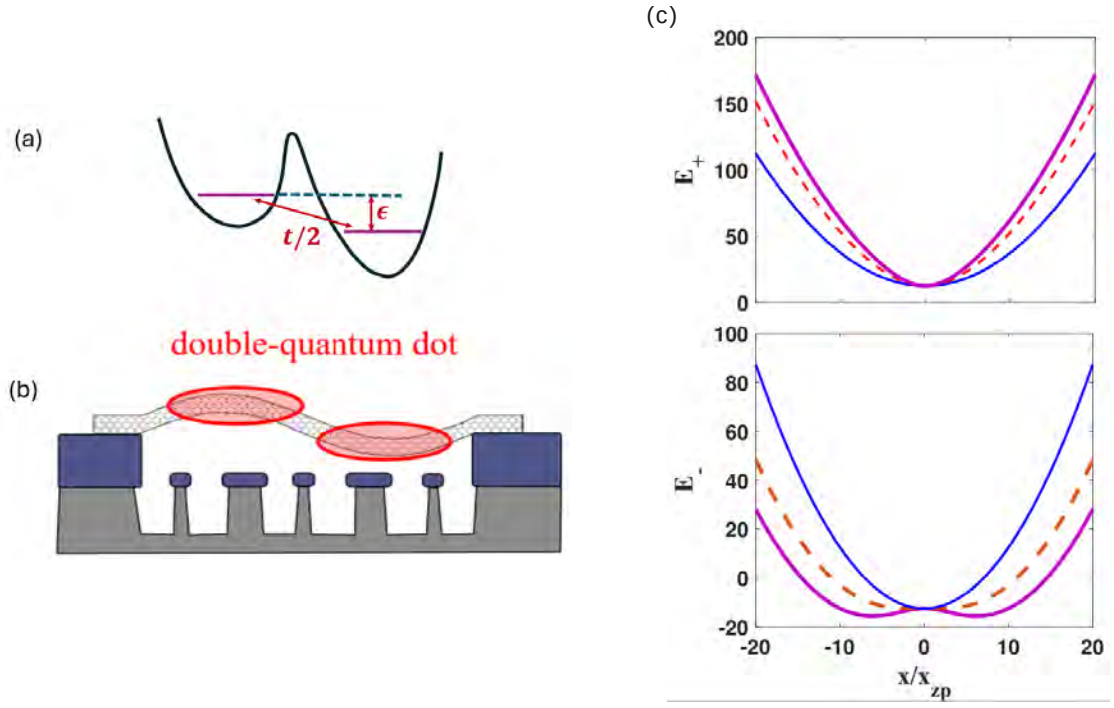

FIG. 5: (a) A schematic of the electronic confinement potential where t is the the hopping amplitude and ϵ is energy difference between the two individual charge states. (b) A schematic of a suspended carbon nanotube which hosts a double quantum dot. It's one-electron charged state is interconnected with the secondary flexural mode. (c) Upper and lower right panels show effective potential for E_+ and E_-, respectively using Eq. (6) for $t/\hbar\omega_0$=20. Here, E_+ and E_- are scaled by $\hbar\omega_0$. Thin solid, dashed and thick solid lines correspond to $4g/\omega_0 = 0, 100$, and 200, respectively.

The experimental validation of the ultrastrong coupling regime and strong anharmonicity represents a significant achievement, as it establishes a foundation for realizing nanomechanical qubits. However, at

low temperatures, the damping rate increases significantly due to the coupling between the resonator and the single quantum dot. The mechanical resonance width in the high temperature limit ($k_BT \gg \hbar g^2/\omega_0$) is given by [35]

$$\Delta\omega = \Gamma_0 + \frac{1}{2}\frac{\hbar g^2}{k_B T}\frac{\omega_0}{\Gamma_e}, \tag{4}$$

where Γ_0 is the damping rate due to other dissipation mechanisms. This charge fluctuation can be minimized by introducing two quantum dots in the resonators. It becomes feasible to define and control a charge qubit embedded in the resonator by adjusting the gate voltages independently for the two quantum dots. Pistolesi *et al* [35] theoretically proposed a possibility of a mechanical qubit by coupling the charge qubit with the second flexural mode in the strong coupling regime as shown in Fig. 5(b).

The Hamiltonian of the system can be described as

$$H = \frac{p^2}{2m} + \frac{m\omega_0^2 x^2}{2} + \frac{\epsilon}{2}\sigma_z + \frac{t}{2}\sigma_x - \hbar g\frac{x}{x_{\rm zp}}\sigma_z \tag{5}$$

where the first two terms correspond to the mechanical mode of frequency ω_0 with effective mass m, displacement x, and momentum p. The second and third terms corresponds to the electronic state of the quantum dots, where the two Pauli matrices σ_z and σ_x represent the dot charge energy splitting and inter-dot charge hopping, respectively. The final term corresponds to the coupling between the vibration and the charge state. This arises physically from the fluctuation of the force exerted on the mechanical mode when the charge transition occurs between the two quantum dots. The magnitude and the polarity of g can be adjusted across a wide range by adjusting the gate voltages. In the semiclassical Born Oppenheimer picture, by diagonalizing the above Hamiltonian, we find the energy eigenvalues as

$$E_\pm(x) = \frac{m\omega_0^2 x^2}{2} \pm \sqrt{\left(\epsilon - 2\hbar g\frac{x}{x_{\rm zp}}\right)^2 + \frac{t^2}{2}}. \tag{6}$$

Considering $\epsilon = 0$ and for small x we can rewrite equation 6 as

$$E_\pm(x) = \pm\frac{t}{2} + \frac{m\omega_0^2}{2}\left(1 \pm \frac{4\hbar g^2}{\omega_0 t}\right)x^2 \mp \frac{4m^2\omega_0^2\hbar^2 g^4}{t^3}x^4. \tag{7}$$

The interaction between the resonator and the double dot results in a renormilization of resonnace frequency and the emergence of quartic and higher-order terms. Figure 5(c) shows that this interaction stiffens the resonant frequency of the upper branch while softens that of the lower one. The quadratic term in Eq. (7) becomes negative if $g > \sqrt{\omega_0 t/4\hbar}$. This results in a double-well potential and bistability akin to what is anticipated for a single quantum dot coupled to a mechanical oscillator. Pistolesi *et al* [35] estimated the quantized energy levels of the system by diagonalizing Eq. (5) numerically. It was shown that for a large value of g, the anharmonicity $a = (\omega_{21} - \omega_{01})/\omega_{01}$ is enough for enabaling quantum control of the qubit

formed by the $|0\rangle$ and $|1\rangle$ state. The anharmonicity about 5% is typically used for a superconducting qubit for full quantum control, where the transition frequencies ω_{01} and ω_{21} are between $|0\rangle$ and $|1\rangle$ states and between $|1\rangle$ and $|2\rangle$, respectively. At very low temperature, the damping originates from the double quantum dots is suppressed exponentially. It is possible to achieve a very high quality factor of the resonator about a few millions. The decoherence of the hybrid system is improved by three oders of magnitude compared to its charge qubit counterpart. It is expected to have sub-kHz decoherence rate in this system. Additionally, mechanical qubits have novel prospects for quantum sensing. Rather than using traditional mechanical resonators to investigate AC forces, it is possible to detect weak DC forces with an exceptional sensitivity down to $\sim 10^{-21} N/\sqrt{Hz}$ [35]. The qubit state can be read out by coupling the system to a microwave superconducting cavity and utilizing a dispersive interaction, similar to the technique used with superconducting qubits.

IV. CONCLUSION

We discussed why a mechanical qubit is not possible to realize with conventional mechanical resonators though it has a remarkable success in preparation of quantum ground state, squeezing, entanglement etc. in a macroscopic objects. We explained the physical origin of the anharmonicity in a carbon nanotube resonator embedded with a quantum dot in detail. Then, we addressed the limitations of a single quantum dot hosted in nanotube the tube. Subsequently, we elaborated the methodology to overcome those limitations by hosting a double quantum dot in the nanotube as prescribed by Pistolesi *et al* [35]. Mechanical qubits may offer new perspectives for quantum sensing and quantum computing.

ACKNOWLEDGEMENTS

C. S. acknowledges the support from Indian Institute of Science Education and Research Bhopal (IISERB).

* Electronic address: csamanta@iiserb.ac.in

[1] M. H. Devoret and R. J. Schoelkopf, Science **339**, 1169 (2013).

[2] F. Arute *et al*, Nature **574**, 505 (2019).

[3] G. Burkard, T. D. Ladd, A. Pan, J. M. Nichol, and J. R. Petta, Rev. Mod. Phys. **95**, 025003 (2023).

[4] J. Yoneda *et al*, Nature nanotechnology **13**, 102 (2018).

[5] N. Hendrickx, W. Lawrie, L. Petit, A. Sammak, G. Scappucci, and M. Veldhorst, Nature communications **11**, 3478 (2020).

[6] C. D. Bruzewicz, J. Chiaverini, R. McConnell, and J. M. Sage, Applied Physics Reviews **6**, 021314 (2019).

[7] M. Ringbauer, M. Meth, L. Postler, R. Stricker, R. Blatt, P. Schindler, and T. Monz, Nature Physics **18**, 1053 (2022).

[8] C. Fluhmann, T. L. Nguyen, M. Marinelli, V. Negnevitsky, K. Mehta, and J. Home, Nature **566**, 513 (2019).

[9] A. Stern and N. H. Lindner, Science **339**, 1179 (2013).

[10] V. Lahtinen and J. Pachos, SciPost Phys. **3**, 021 (2017).

[11] B. Yang, H. Sun, C.-J. Huang, H.-Y. Wang, Y. Deng, H.-N. Dai, Z.-S. Yuan, and J.-W. Pan, Science **369**, 550 (2020).

[12] H.-N. Dai, B. Yang, A. Reingruber, X.-F. Xu, X. Jiang, Y.-A. Chen, Z.-S. Yuan, and J.-W. Pan, Nature Physics **12**, 783 (2016).

[13] M. W. Doherty, N. B. Manson, P. Delaney, F. Jelezko, J. Wrachtrup, and L. C. Hollenberg, Physics Reports **528**, 1 (2013).

[14] F. Jelezko and J. Wrachtrup, physica status solidi (a) **203**, 3207 (2006).

[15] S. Pezzagna and J. Meijer, Applied Physics Reviews **8**, 011308 (2021).

[16] H. G. Craighead, Science **290**, 1532 (2000).

[17] K. Ekinci and M. Roukes, Rev. Sci. Instrum. **76**, 061101 (2005).

[18] M. Roukes, Physics World **14**, 25 (2001).

[19] A. D. O'Connell *et al*, Nature **464**, 697 (2010).

[20] J. D. Teufel, T. Donner, D. Li, J. W. Harlow, M. Allman, K. Cicak, A. J. Sirois, J. D. Whittaker, K. W. Lehnert, and R. W. Simmonds, Nature **475**, 359 (2011).

[21] J. M. Pirkkalainen, E. Damskagg, M. Brandt, F. Massel, and M. A. Sillanpaa, Phys Rev Lett **115**, 243601 (2015).

[22] M. Rossi, D. Mason, J. Chen, Y. Tsaturyan, and A. Schliesser, Nature **563**, 53 (2018).

[23] E. E. Wollman, C. U. Lei, A. J. Weinstein, J. Suh, A. Kronwald, F. Marquardt, A. A. Clerk, and K. C. Schwab, Science **349**, 952 (2015).

[24] J. Suh, A. J. Weinstein, C. U. Lei, E. E. Wollman, S. K. Steinke, P. Meystre, A. A. Clerk, and K. C. Schwab, Science **344**, 1262 (2014).

[25] C. F. Ockeloen-Korppi, E. Damskagg, J. M. Pirkkalainen, A. A. Clerk, M. J. Woolley, and M. A. Sillanpaa , Phys. Rev. Lett. **117**, 140401 (2016).

[26] S. Kotler *et al*, Science **372**, 622 (2021).

[27] E. A. Wollack, A. Y. Cleland, R. G. Gruenke, Z. Wang, P. Arrangoiz-Arriola, and A. H. Safavi-Naeini, Nature **604**, 463 (2022).

[28] R. W. Andrews, R. W. Peterson, T. P. Purdy, K. Cicak, R. W. Simmonds, C. A. Regal, and K. W. Lehnert, Nature physics **10**, 321 (2014).

[29] K. Fang, M. H. Matheny, X. Luan, and O. Painter, Nature Photonics **10**, 489 (2016).

[30] A. Reed *et al*, Nature Physics **13**, 1163 (2017).

[31] R. Lifshitz and M. C. Cross, Reviews of nonlinear dynamics and complexity, **Chapter 1** (2008).

[32] H. W. C. Postma, I. Kozinsky, A. Husain, and M. L. Roukes, Appl. Phys. Lett. **86**, 223105 (2005).

[33] S. Rips and M. J. Hartmann, Phys. Rev. Lett. **110**, 120503 (2013).

[34] S. Rips, I. Wilson-Rae, and M. Hartmann, Phys. Rev. A **89**, 013854 (2014).

[35] F. Pistolesi, A. N. Cleland, and A. Bachtold, Phys. Rev. X **11**, 031027 (2021).

[36] C. Samanta *et al*, Nature Physics **19**, 1340 (2023).

[37] R. G. Knobel and A. N. Cleland, Nature **424**, 291 (2003).

[38] B. Lassagne, Y. Tarakanov, J. Kinaret, D. Garcia-Sanchez, and A. Bachtold, Science **325**, 1107 (2009).

[39] G. A. Steele, A. K. Huttel, B. Witkamp, M. Poot, H. B. Meerwaldt, L. P. Kouwenhoven, and H. S. J. van der Zant, Science **325**, 1103 (2009).

[40] Y. Okazaki, I. Mahboob, K. Onomitsu, S. Sasaki, and H. Yamaguchi, Nature Communications **7**, 11132 (2016).

[41] I. Khivrich, A. A. Clerk, and S. Ilani, Nature Nanotechnology **14**, 161 (2019).

[42] C. Urgell, W. Yang, S. L. De Bonis, C. Samanta, M. J. Esplandiu, Q. Dong, Y. Jin, and A. Bachtold, Nature Physics **16**, 32 (2020).

[43] Y. Wen, N. Ares, F. J. Schupp, T. Pei, G. A. D. Briggs, and E. A. Laird, Nature Physics **16**, 75 (2020).

[44] S. Blien, P. Steger, N. Hittner, R. Graaf, and A. K. Huttel, Nature Communications **11**, 1636 (2020).

[45] C. Samanta, D. Czaplewski, S. De Bonis, C. Moller, R. Tormo-Queralt, C. Miller, Y. Jin, F. Pistolesi, and A. Bachtold, Appl. Phys. Lett. **123**, 203502 (2023).